

See discussions, stats, and author profiles for this publication at: <https://www.researchgate.net/publication/282910745>

Bio-Inspired Smart Gate-Location-Controllable Single Nanochannels: Experiment and Theoretical Simulation

ARTICLE *in* ACS NANO · OCTOBER 2015

Impact Factor: 12.88 · DOI: 10.1021/acsnano.5b05542

READS

50

8 AUTHORS, INCLUDING:



Huacheng Zhang

Technical Institute of Physics and Chemistry

22 PUBLICATIONS 275 CITATIONS

[SEE PROFILE](#)



Jue Hou

Chinese Academy of Sciences

10 PUBLICATIONS 44 CITATIONS

[SEE PROFILE](#)



Xu Hou

Harvard University

31 PUBLICATIONS 1,407 CITATIONS

[SEE PROFILE](#)



Guanglei Hou

Chinese Academy of Sciences

7 PUBLICATIONS 51 CITATIONS

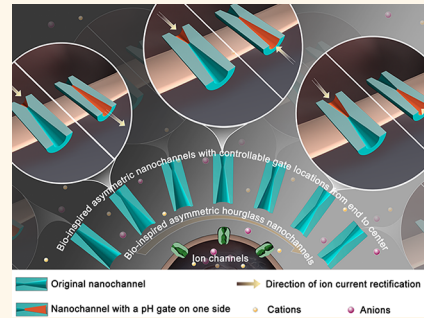
[SEE PROFILE](#)

Bioinspired Smart Gate-Location-Controllable Single Nanochannels: Experiment and Theoretical Simulation

Huacheng Zhang,^{*†} Ye Tian,[‡] Jue Hou,[‡] Xu Hou,[‡] Guanglei Hou,[‡] Ranwen Ou,[§] Huanting Wang,[§] and Lei Jiang^{*†}

[†]Laboratory of Bio-Inspired Smart Interfacial Science, Technical Institute of Physics and Chemistry, Chinese Academy of Sciences, Beijing 100190, People's Republic of China, [‡]Beijing National Laboratory for Molecular Sciences, Key Laboratory of Organic Solids, Institute of Chemistry, Chinese Academy of Sciences, Beijing, 100190, People's Republic of China, and [§]Department of Chemical Engineering, Monash University, Clayton, Victoria 3800, Australia

ABSTRACT pH-activated gates intelligently govern the ion transport behaviors of a wide range of bioinspired ion channels, but the mechanisms between the gate locations and the functionalities of the ion channels remain poorly understood. Here, we construct an artificial gate-location-tunable single-nanochannel system to systematically investigate the impact of the gate location on the ion transport property of the biomimetic ion channel. The gate-location-controllable single nanochannels are prepared by asymmetrically grafting pH-responsive polymer gates on one side of single nanochannels with gradual shape transformation. Experimental ion current measurements show that the gating abilities and rectification effects of the pH-gated nanochannels can be gradually altered by precisely locating the artificial pH gates on the different sites of the channels. The experimental gate-location-dependent gating and rectification of ion current in the bioinspired ion channel system is further well confirmed by theoretical simulation. This work, as an example, provides a new avenue to optimize the smart ion transport features of diverse artificial nanogate devices *via* precisely locating the gates on the appropriate sites of the artificial nanochannels.



KEYWORDS: bioinspired ion channel · pH gating · ion current rectification · single nanochannel · tunable gate location

Ion channels, which intelligently control movements of ions and molecules into and out of cells through their unique nanostructures and functional stimuli-triggered gates,¹ provide a big source of bio-inspiration for scientists to build robust and stable artificial smart nanochannel materials with a wide range of applications in nanofluidic logic devices,^{2–9} molecule filters,^{10–14} and biosensors.^{15–22} From the structure way, a series of symmetrically and asymmetrically shaped solid-state nanochannels have been prepared to exhibit the shape-dependent symmetric and asymmetric ion transport properties analogous to biological ion channels. For instance, asymmetrically cone-^{23,24} and bullet-shaped²⁵ nanochannels have been fabricated to realize the ion current rectification properties that were originally discovered in the biological rectifier ion channels. The symmetrically cylinder-,²⁶ hourglass-,⁴ and cigar-shaped^{27,28} nanochannels have been confirmed to show symmetric current–voltage properties.

On the other hand, in order to further enhance the functionalities of the bio-inspired nanochannels, the synthetic symmetrically and asymmetrically shaped nanochannels have been modified with various kinds of artificial functional gates to realize the smart gating functions found in the biological ion channels.^{29–31} The artificial gates of the bioinspired ion channels were generally made by smart responsive molecules, such as pH-,^{32–38} light-,^{39–42} thermo-,^{43–45} and ion-sensitive molecules.^{46–50} These functional molecules immobilized on the inner surfaces of the bioinspired channels could reversibly change their conformations between different states. Some of the conformational states allow the channels to conduct certain ions, while others prohibit the ionic transport through the channels. Reversibly conformational transition of the synthetic nanochannel between these different ion transport states is usually referred to as gating. To date, although various advanced symmetric and asymmetric

* Address correspondence to
zhanghc@mail.ipc.ac.cn,
jianglei@iccas.ac.cn.

Received for review September 3, 2015
and accepted October 16, 2015.

Published online
10.1021/acsnano.5b05542

© XXXX American Chemical Society

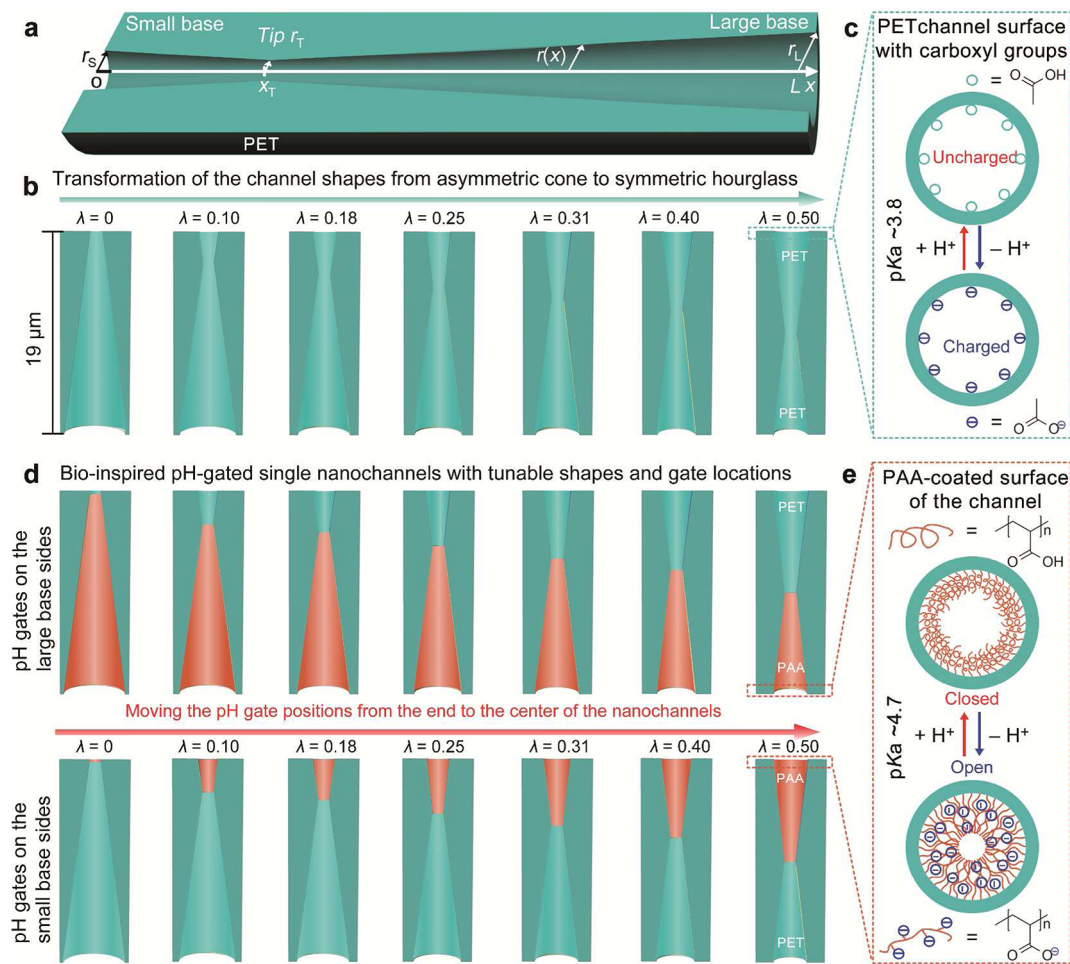
modification methods⁵¹ allow scientists to achieve diverse symmetric and asymmetric gating of bio-inspired ion channel systems, the influence of the gate locations on the ion transport properties in these bioinspired channels remains poorly understood. Moreover, the gate-location-dependent ion transport features have been widely found in biological ion channels,¹ such as the inward rectifier potassium channel;^{52,53} its pH-gating and rectifying behaviors are mostly dependent on the location of the leucine gate.⁵⁴ By repositioning the leucine gate on the different sites of the channel, the rectifying behavior and pH-gating ability of the channel were altered strongly. The channel exhibited the highest ion rectification and pH gating effects only when the leucine gate was located at a site near the selectivity filter.

Herein, inspired by the inward rectifier potassium channel, we construct the bioinspired gate-location-controllable nanochannels for the first time to systematically study the gate-location-dependent ion transport behaviors of the bioinspired ion channels. The single nanochannels whose gate locations can be gradually changed from the channel end to the channel center are prepared by asymmetrically grafting artificial pH gates on different sites of the shape-tunable asymmetric hourglass nanochannels. Through grafting the pH gates onto the small or large base sides of the nanochannels, two kinds of gate-location-controllable nanochannels, including the nanochannels with the pH gates on the small base sides and the nanochannels with the pH gates on the large base sides, can be obtained, respectively. These two kinds of nanochannels exhibit very different gate-location-dependent pH-gating and rectification characteristics. The pH-gating and rectification effects of the channels with the pH gates on the small base sides are enhanced differently, while the rectification properties of the channels with the pH gates on the large base sides are weakened and even reversed with changes in the position of the pH gate from the channel end to the channel center. Additional simulation results well confirm that the gate-location-dependent enhancement and inversion of the transport behaviors of the nanochannels are attributed to the cooperation and competition between their asymmetric geometries and gate-location-induced asymmetric surface properties.

As shown in Scheme 1, the single asymmetric hourglass nanochannels are used to construct the bioinspired gate-location-controllable ion channels owing to their tunable geometries. Scheme 1a shows an asymmetric hourglass nanochannel that has a very small opening inside the channel and two different large openings at its two ends. The small opening inside the channel was called “tip”, while the large openings of the channel were called “small base” and “large base” in accordance with their sizes, respectively. As illustrated in Scheme 1b, seven representative

asymmetric hourglass nanochannels with tunable shape asymmetries were fabricated through asymmetric chemical etching⁵⁵ of single-track polyethylene terephthalate (PET) membranes (see Text S1 and Figure S1, Supporting Information (SI)). To well distinguish these differently shaped nanochannels, the non-dimensional tip position (λ), which is equal to the tip position (x_T) divided by the whole length (L) of the nanochannel, $\lambda = x_T/L$, was used to represent the nanochannels (Scheme 1a). Tip positions of the nanochannels were experimentally obtained by characterization of their cross sections (Text S2, SI), and average λ values of the seven typical nanochannels were 0, 0.10, 0.18, 0.25, 0.31, 0.40, and 0.50, respectively (Scheme 1b). Each nanochannel with an individual λ was marked as nanochannel λ (N λ). The changing tip positions of the seven nanochannels led to a gradual transformation of the geometries from asymmetric conical shape to symmetric hourglass shape. In addition, because the cleavage of the PET chains during chemical etching could produce pH-responsive carboxyl groups on the inner surfaces of the PET nanochannels,⁵⁶ the surface of the PET channel was electrically neutral when the pH was below the pK_a of 3.8⁵⁷ and negatively charged when the pH was above the pK_a (Scheme 1c).

After obtaining the shape-tunable single nanochannels, two kinds of gate-position-controllable nanochannels could be fabricated by selectively locating an artificial pH gate on the small or large base sides of the nanochannels with the seven typical structures. One kind is the nanochannels with pH gates located on the large base sides (Scheme 1d, up); the other kind is the nanochannels with pH gates located on the small base sides (Scheme 1d, down). The locating positions of the pH gates of these two kinds of nanochannels could be continuously altered from the channel end to the channel center when the channel shapes were gradually transformed from the conical shape to the symmetric hourglass shape (Scheme 1c, from left to right). A pH-responsive polyelectrolyte, poly(acrylic acid) (PAA), was used here to be the artificial pH gate of the bioinspired nanochannel system, because PAA brushes could undergo pH-responsive conformational transitions between the collapsed, neutral, and hydrophobic state when the pH was below the pK_a of 4.7 and the swollen, negatively charged, and hydrophilic state when the pH was above the pK_a .⁵⁸ The pH-responsive conformational conversions of the PAA brushes on the inner surface of the channel led the surface charge, the wettability, and the effective size of the channel changing with the environmental pH variation, thus forming the open and closed states of the channel (Scheme 1e). As a result, with the PAA gate positions of the two kinds of artificial ion channels gradually changing from the channel end to the channel center, ion channels with pH gates respectively on the small and large base sides would exhibit different pH-gating ion



Scheme 1. Design strategy of the single nanochannels with tunable gate locations. (a) Schematic representation of an asymmetric hourglass nanochannel with geometric parameters, including small base radius (r_s), tip radius (r_t), large base radius (r_l), length of channel (L), tip position (x_t), and radius profile ($r(x)$). (b) Structures of the asymmetric hourglass nanochannels gradually transform from asymmetric to symmetric. (c) pH-responsive property of carboxyl groups on the inner surface of the original PET nanochannel between the charged and uncharged states. (d) Two kinds of gate-position-controllable nanochannels with the pH gates (indicated by orange color) on the small and large base sides, respectively. The locations of the pH gates of the two kinds of nanochannels are continuously varied from the channel end to the channel center. (e) PAA brushes underwent reversible pH-responsive conformational transitions between the collapsed, neutral, hydrophobic state (up) and the swollen, negatively charged, hydrophilic state (down), leading to closed and open states of the channel, respectively.

transport properties, and the directions and degrees of ion current rectification in these two kinds of ion channels would be gradually tuned.

RESULTS AND DISCUSSION

Scanning electron microscopy (SEM) images of the small and large base sides of the seven representative asymmetric hourglass nanochannels well illustrated their gradual shape transformation, and the narrow tips inside the nanochannels can be seen easily and clearly from the SEM images of their small and large base sides. The radii of the small and large bases were studied and analyzed from multichannel membranes prepared under the same conditions as single channel membranes by SEM, due to the difficulty of locating the small and large base sides of the single nanochannel membranes in SEM for the efficient shape analysis of

the seven representative nanochannels. Statistic results of the average radii of the small and large bases of the channels with relevant standard deviations are shown in Table S2 in the SI. With λ increasing from 0 to 0.50, the small base radii of the channels increased from ~ 3 nm to ~ 313 nm, while the large base radii decreased from ~ 643 nm to ~ 313 nm, until the two radii became equal at $\lambda = 0.50$. Because the tips located on the cross sections of the channels were too small to experimentally measure, the tip radii of the asymmetric hourglass nanochannels could be calculated by eq 1,⁵⁵ where k is the specific conductivity of a 1 M potassium chloride (KCl) solution (pH 2.8, $k = 11.13 \Omega^{-1} \text{ m}^{-1}$ at 25 °C), L is the length of the nanochannel ($L = 19 \mu\text{m}$), λ is the nondimensional tip position of the channel, and G_0 is the conductance value of the channel at the 1 M KCl solution. The conductance values of the

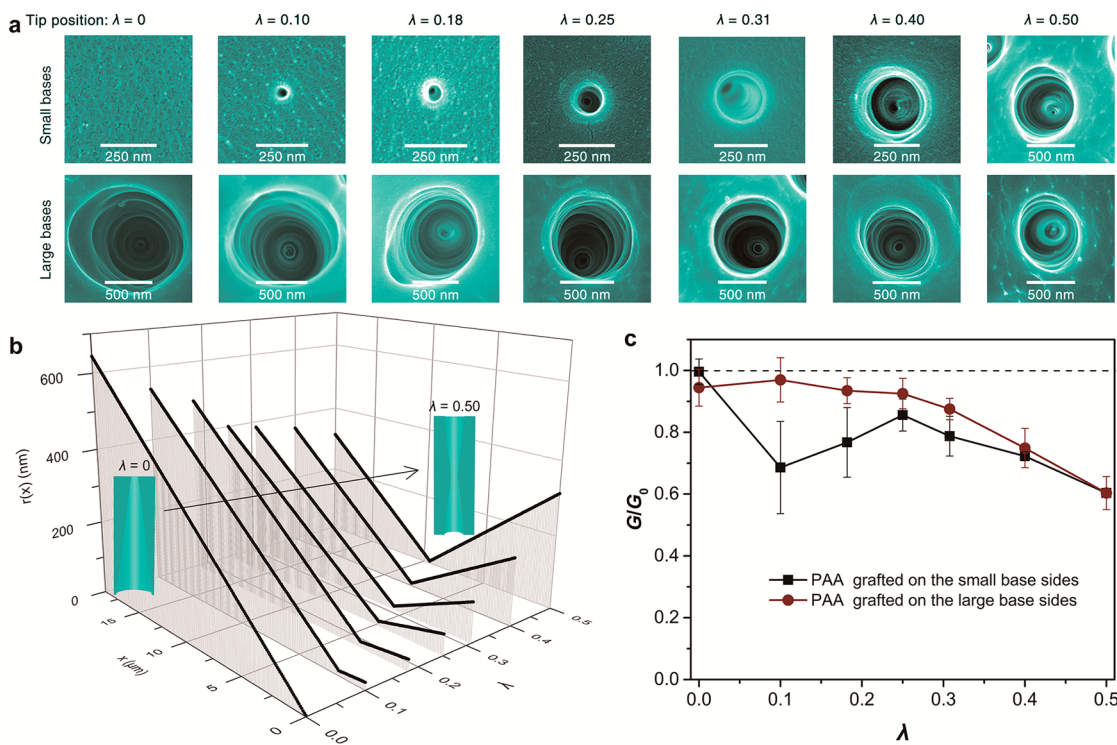


Figure 1. Fabrication and modification of the asymmetric hourglass nanochannels. (a) SEM images of the small and large base sides of the seven representative asymmetric hourglass nanochannels N_0 , $N_{0.10}$, $N_{0.18}$, $N_{0.25}$, $N_{0.31}$, $N_{0.40}$, and $N_{0.50}$. The narrow tips inside the nanochannels can be seen easily and clearly from the SEM images. It is worth mentioning that the small base of the channel (N_0) on the membrane surface is too small to be observed by SEM. (b) Radius profiles of the seven representative asymmetric hourglass nanochannels well demonstrate the gradual transformation of the channel shapes. (c) Relative conductance value changes (G/G_0) of the nanochannels before and after modification in a 1 M KCl solution.

channels were determined by fitting the slope of the transmembrane ion current as a function of the applied voltage. The numerical results showed that the tip radii of the channels remained around 10 nm (Table S2 in the SI). After observing all geometrical parameters of the asymmetric single nanochannels (Table S2 in the SI), radius profiles $r(x)$ of the seven asymmetric hourglass nanochannels N_0 , $N_{0.1}$, $N_{0.18}$, $N_{0.25}$, $N_{0.31}$, $N_{0.4}$, and $N_{0.5}$ could be theoretically described by eq 2, where r_s , r_t , and r_l are respectively the radii of the small base, tip, and large base, x_t is the tip position, and L is the channel length. As shown in Figure 1b, theoretical radius profiles of the seven single nanochannels well confirmed the gradual transformation of their geometries from an asymmetric conical shape to a symmetric hourglass shape.

$$r_t = \frac{LG_0}{\pi k} \left(\frac{\lambda}{r_s} + \frac{1-\lambda}{r_l} \right) \quad (1)$$

$$r(x) = \begin{cases} r_s - \frac{r_s - r_t}{x_t} x, & x \leq x_t \\ r_t + \frac{r_l - r_t}{L - x_t} (x - x_t), & x > x_t \end{cases} \quad (2)$$

PAA brushes were asymmetrically located on the small or large base sides of the asymmetric hourglass nanochannels by a well-developed plasma-induced polymerization method (see Text S3 in the SI).⁵⁸ During the

plasma treatment, because the narrowest tip inside the channel could effectively prevent monomers from diffusing into the other side of the channel, the PAA brushes were asymmetrically grafted on the side treated by plasma modification. The narrowest tip was the transition point of the modified and the unmodified region of the channel. As a result, through plasma treatment of the small base sides of the seven representative nanochannels with tunable tip positions, seven artificial ion channels with the PAA gates on their small base sides could be prepared, and the gate positions of the channels were gradually varied from the channel end to the channel center (Scheme 1d, down). In the same way, another seven gate-position-controllable ion channels whose PAA gates were deposited on the large base sides could be obtained (Scheme 1d, up). To further confirm whether the PAA brushes were grafted on one side of the nanochannels, conductance values of the single nanochannels before and after modification were systematically measured in 1 M KCl (pH 2.8). The conductance values of the channels were determined by fitting the slope of the transmembrane ion current as a function of the applied voltage (see Figure S3 in the SI). In this work, we fabricated at least four samples of each kind of single nanochannel to obtain the average conductance changes of the channel before and after modification.

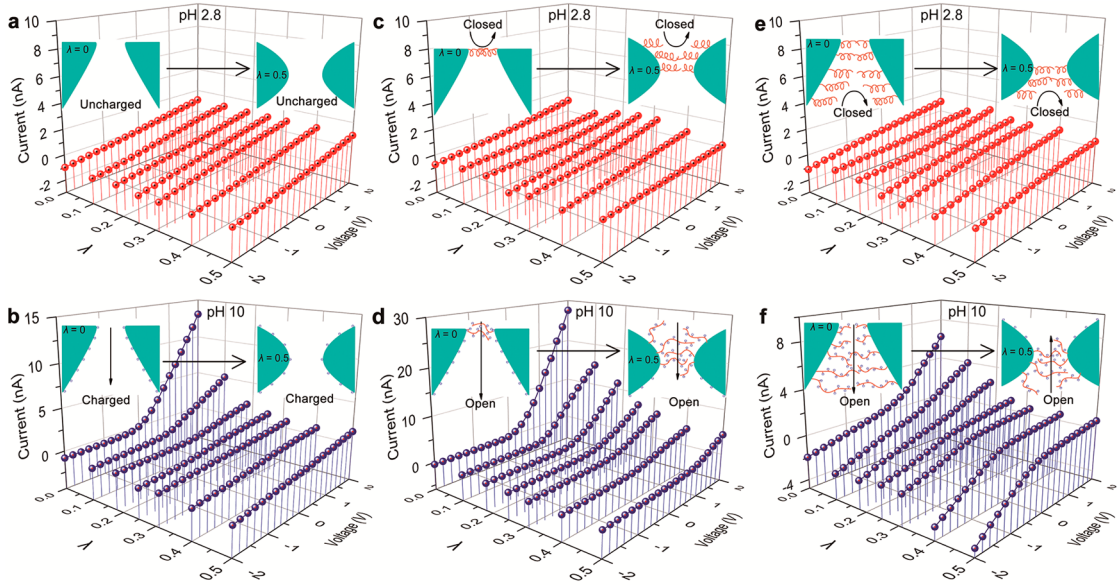


Figure 2. I – V curves and corresponding surface properties of the shape-tunable single nanochannels (a, b) before and after grafting PAA brushes on the (c, d) small and (e, f) large base sides under pH 2.8 and pH 10 conditions. The black arrows are used to indicate the preferential ion transport directions in the single nanochannels.

Before modification, the conductance values of all single nanochannels (G_0) were controlled around 3.5 nS. After modification, the conductance values of the nanochannels (G) were decreased due to the grafted polymer layers on the inner walls of the channels. As shown in Figure 1c, the ratios (G/G_0) of the nanochannels were below 1, confirming that the PAA gates were successfully grafted on the small or large base sides of the channels.

In order to well demonstrate the gate-location-controlled ion transport behaviors inside the bioinspired pH-gated ion channels, the ion transport properties of the nanochannels before and after modification were systematically investigated by measuring the transmembrane ionic currents of the nanochannels in 0.1 M KCl solutions with different pH values. As shown in Figure 2a, although the shapes of the seven original PET nanochannels were altered from asymmetric to symmetric, they exhibited similar symmetric I – V curves under pH 2.8 condition. All of the nanochannels were electrically neutral when the pH was below a pK_a of 3.8 (Figure 2a, inset). At high pH, the walls of the channels were negatively charged (Figure 2b, inset), and the uniformly charged nanochannels exhibited varied nonlinear I – V curves under pH 10 condition (Figure 2b), because the asymmetrical geometry of the negatively charged nanochannel could induce a preferential direction for ions transporting from the small to large base side. In detail, the initial three nanochannels N_0 , $N_{0.10}$, and $N_{0.18}$ demonstrated asymmetric I – V curves under pH 10 condition, and the asymmetry of the I – V curves decreased gradually with increasing channel-shape symmetry. As the shape continuously evolved from asymmetric hourglass to symmetric hourglass,

the latter four nanochannels $N_{0.25}$, $N_{0.31}$, $N_{0.40}$, and $N_{0.50}$ all illustrated nearly symmetric I – V curves under pH 10 condition. It turned out that the ion transport properties of the uniformly charged nanochannels could be gradually tuned from asymmetric to symmetric by controlling the channel shape asymmetry.

After grafting the PAA brushes on the small base sides of the nanochannels, the surface properties of the nanochannels became asymmetric. The small base sides of the channels were coated with PAA chains, while the unmodified large base sides were still coated with carboxyl groups. Under pH 2.8 condition, the PAA gates on the small base sides were closed and carboxyl groups on the unmodified large base sides were neutral. So the modified nanochannels were uncharged at pH 2.8 (Figure 2c, inset). As a result, the nanochannels also exhibited nearly linear I – V curves under pH 2.8 condition. However, when the pH increased to 10, the PAA gates on the small base sides of the nanochannels were switched to the open states and the carboxyl groups on the unmodified large base sides of the nanochannels became negatively charged. Due to the highly charged PAA brushes on the modified small bases sides of the channels, the surface charge densities of the PAA-modified small base sides of the channels were larger than the charge densities of the unmodified large base sides (Figure 2d, inset). These surface charge gradients from the small to large base sides of the nanochannels further enhanced their asymmetric ion transport properties. Thus, much more asymmetric I – V curves of the channels were obtained under pH 10 condition (Figure 2d). The asymmetries of the I – V curves decreased with transformation of gate positions from the channel end to the channel center because

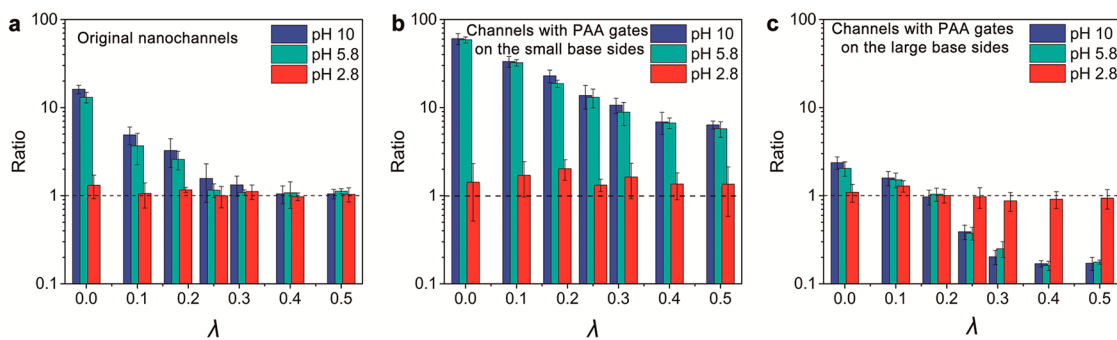


Figure 3. Average ICR ratios of (a) the original and the modified nanochannels with the PAA gates on the (b) small and (c) large sides under pH 2.8, pH 5.8, and pH 10 conditions at 2 V. Ratio = $I_{+2V}/|I_{-2V}|$.

both the channel shape asymmetries and the surface charge gradients decreased with the gate position changes.

For the nanochannels with the PAA gates on the large base sides, they were uncharged as well and showed almost linear $I-V$ curves under pH 2.8 condition (Figure 2e). However, they exhibited very different ion transport properties under pH 10 condition (Figure 2f) because their surface charge gradients were from the large to small base sides on the open states, which was opposite the shape asymmetries of the channels (Figure 2f, inset). Therefore, the ion transport properties of the nanochannels with the PAA gates on the large base sides depended on the competition between the surface charge gradient (from large to small side) and the shape asymmetry (from small to large side) under open states. With increasing λ from 0 to 0.50, the shape asymmetries of the nanochannels decreased gradually, while the asymmetries of the surface charge distributions were enhanced gradually. When λ was below 0.18, the surface charge gradient was smaller than the shape asymmetry; hence the nanochannels N_0 and $N_{0.10}$ still showed asymmetric $I-V$ curves with preferential ion transport direction from the small to large base sides. Moreover, when λ reached 0.18, the surface charge gradient was similar to the shape asymmetry. Consequently, channel $N_{0.18}$ showed a nearly symmetric $I-V$ property. However, when λ was above 0.18, the surface charge gradient was larger than the geometry asymmetry. Hence the preferential ion transport directions of the nanochannels $N_{0.25}$, $N_{0.31}$, $N_{0.40}$, and $N_{0.50}$ were reversed, and the preferential directions were from the large to small base sides (Figure 2f). Therefore, under the open states, the ion transport features of the artificial pH-gating nanochannels were altered strongly by changing the locations of the artificial pH gates.

More intuitionistic contrast of the asymmetric ion transport properties between the original and modified nanochannels was further illustrated by the degree of ion current rectification (ICR). The ICR degree was defined as the ratio of absolute values of ion currents recorded at a given positive voltage (+2 V,

ion current flows from the small to the large base side of the channel) and at the same absolute value of a negative voltage (-2 V, ion current flows from the large to the small base side of the channel); ratio = $I_{+2V}/|I_{-2V}|$. The ICR ratios of the nanochannels were tested under three representative (pH 2.8, pH 5.8, and pH 10) conditions. The mean ICR ratio of each kind of nanochannel before and after modification was averaged from at least three reproduced samples. As shown in Figure 3, under pH 2.8 condition, the average ICR ratios of all nanochannels were kept around 1, which indicated that the channels either before or after modification could not rectify ions under the acid condition. When the pH was above the pK_a of PAA, the ICR ratios of the original and the functionalized channels became very different, and the ICR ratios of the nanochannels under pH 5.8 condition were almost the same as those at pH 10 condition. Before modification, the rectification ratios of the original nanochannels decreased rapidly from ~16.1 to ~3.2 under pH 10 condition at the beginning and remained around 1 because λ reached a value of 0.25 (Figure 3a). After asymmetric PAA modification, the rectification ratios of the channels with the PAA gates on the small base sides were much higher than those of the original channels (Figure 3b), whereas rectification ratios of the channels with the PAA gates on the large base sides were lower than those of the original channels (Figure 3c). Under pH 10 condition, with the PAA gate position increasing from 0 to 0.50, the rectification ratios of the nanochannels with the PAA gates on the small base sides consistently decreased from ~60.6 to ~6.3 (Figure 3b), while the ratios of the nanochannels with the PAA gates on large base sides gradually reduced from ~2.37 to ~0.17 (Figure 3c). When the rectification ratio was below 1, the direction of the ion current rectification inside the nanochannels with the PAA gates on the large base sides was reversed (Figure 3c).

To obtain a comprehensive understanding of the shape asymmetry and the gate position cooperatively controlled pH-gating ICR effects of the gate-location-tunable nanochannels, we further used a continuous theory based on Poisson–Nernst–Planck (PNP)

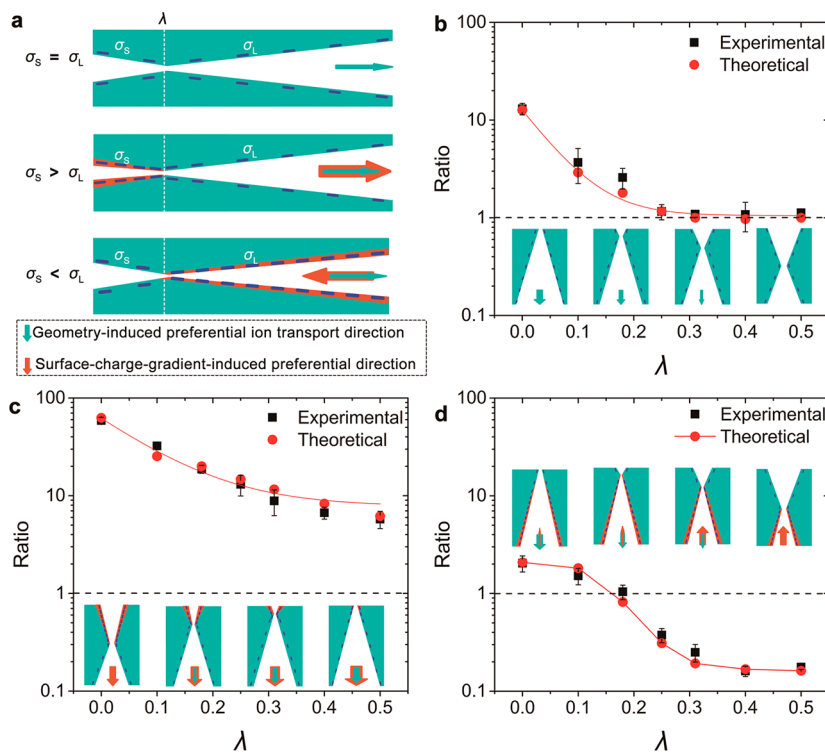


Figure 4. Theoretical simulation. (a) Simplified schemes of the asymmetric hourglass nanochannels before and after modification for theoretical simulation. The cyan arrows are used to indicate the shape-asymmetry-induced preferential ion transport direction of the nanochannel, while the orange arrows are used to indicate the surface-charge-gradient-induced preferential ion transport direction of the nanochannel. (b–d) Comparison of the experimental and theoretical ICR ratios of (b) the original and the modified nanochannels with the PAA gates on the (c) small and (d) large base sides under pH 5.8 conditions at 2 V. The insets are schematic illustrations of the nanochannels before and after asymmetric PAA modification that exhibit shape and gate-location cooperative ion transport properties.

equations;^{59–61} see Text S4 in the SI for a detailed discussion of the theoretical calculation. In order to avoid complex calculation processes, here we are mainly concerned with the effects of the shape and the surface charge density and distribution of the channels on their ion transport properties. The influences of the channel size and wettability variations of the PAA gates on the ionic transport properties were neglected in accordance with previous works.^{35,61,62} As a result, the PAA-asymmetric-modified nanochannels could be simplified to a nanofluidic system where charges distributed on the polymer brushes were strictly confined to the nanochannel walls (Figure 4a). Before modification, because the whole inner surface of the PET nanochannels is uniformly covered by the carboxylate groups, the surface charge density of the small base side (σ_s) is equal to the surface charge density of the large base side (σ_L) under the charged states of the nanochannels (Figure S4a, SI). The shape asymmetries are the key factors to control the ion transport properties of the channels, and the shape-asymmetry-induced preferential ion transport directions of the channels are from the small to large base sides of the channels (Figure 4b, inset). However, after PAA asymmetric modification, the surface charge densities of the channels become inhomogeneous (Figure 4a). For the channels with the PAA gates on

the small base sides, due to the highly charged PAA brushes on the small base sides of the nanochannels, σ_s is larger than σ_L under the charge state (Figure S4b, SI). The directions of the surface charge gradients of the nanochannels (from small to large side) are the same as the directions of the shape asymmetries of the nanochannels (Figure 4c, insets). So the rectification properties of the nanochannels are enhanced by cooperation of the shape-asymmetry-induced and the surface-charge-gradient-induced ion transport. For the nanochannels with the PAA gates on the large base sides, σ_s is smaller than σ_L (Figure S4c, SI). The directions of the surface charge gradients of the channels are opposite the directions of the shape asymmetries of the channels. The rectification directions and degrees inside these nanochannels are dependent on competition between the shape asymmetries and the surface charge gradients (Figure 4d, insets).

On the basis of the three different models of the nanochannels before and after modification shown in Figure 4a and the parameters shown in Table S3, we systematically calculated ion transport properties of the nanochannels before and after modification under pH 2.8 and pH 5.8 conditions. Theoretically calculated ICR ratios of the nanochannels before and after modification under pH 2.8 condition were around 1, which

was well consistent with the experimental results (Figure S8, SI). Furthermore, the theoretical ICR ratios of the nanochannels before and after modification under pH 5.8 condition also showed excellent agreement with the experimental observations. Before modification, both experimental and theoretical results illustrated that the ICR ratios of the nanochannels decreased gradually from ~ 12.7 to ~ 1.0 when channel shapes varied from asymmetric cone to symmetric hourglass (Figure 4b). After modification, with the gate position increasing from 0 to 0.50, both experimental and theoretical ICR ratios of the nanochannels with the PAA gates on the small base sides consistently decreased from ~ 60.0 to ~ 6.0 (Figure 4c), whereas the experimental and theoretical ICR ratios of the nanochannels with the PAA gates on the large base sides decreased from ~ 2.08 to ~ 0.17 (Figure 4d). These results further confirmed that the ICR degrees of the channels with the PAA gates asymmetrically located on the small base sides were much stronger than those of the channels with the PAA gates on the large bases sides despite the variations of the gate locations of the channels. Therefore, the experimental gate-position-dependent and pH-responsive ICR effects could be rationally expected by the PNP equations, and the location of the PAA gate was confirmed as an important factor to control the ion transport properties of the bioinspired nanochannels through changing the surface charge distributions of the nanochannels. However, although the PNP theory nearly quantitatively predicted the experimental results in this work, using the PNP theory to predict the polymer chain modified nanochannel system still had many limitations, namely, that it did not consider the impacts of the conformational behavior of the polymers, van der Waals and repulsive interactions of the charged polymers, and wettability on the ion transport properties of the nanochannel. For these reasons, developing a new theoretical framework to simulate the

polymer-asymmetric-modified nanochannel system remains an important research direction.

CONCLUSION

In summary, we have experimentally and theoretically demonstrated a bioinspired gate-position-controllable nanochannel system *via* asymmetrically locating the PAA gates on different sites of the shape-tunable single asymmetric hourglass nanochannels. With the locations of the PAA gates gradually changing from the channel end to the channel center, the PAA-functionalized single nanochannels displayed very different gate-position-dependent ion transport features. The nanochannels with the PAA gates on the small base sides exhibited very strong gating and rectification properties, while the gating abilities and rectification effects of the nanochannels were weakened and even reversed when the PAA gates were oppositely located on the large base sides of the channels. The experimentally observed multifunctional gate-location-dependent ion transport properties were further theoretically proved by the PNP theory. It has been proved that the gate-location-induced enhancement and inversion of the ion gating and rectification are attributed to the cooperation and competition between asymmetric geometries and the gate-position-controlled asymmetric surface charge distributions of the nanochannels. Therefore, both experimental and theoretical findings in this work have given a comprehensive understanding of the mechanism between the gate locations and the functionalities of the nanochannels. As a novel artificial gate-position-controllable nanochannel system, it may display the advanced feature of providing a novel bioinspired strategy to develop new high-sensitive nanogates for biosensing, to design new ultrahigh ion-rectifying membranes for energy conversions, and to construct new bioinspired ultrafast water transport nanochannel membranes for seawater desalination.

EXPERIMENTAL SECTION

Materials. PET membranes of 19 μm thickness (Hostaphan RN 19, Hoechst) were irradiated at the linear accelerator UNILAC (GSI, Darmstadt) with swift heavy ions (Pb, U, or Au) having an energy of 11.4 MeV per nucleon. Sodium hydroxide (NaOH, 96%), potassium chloride (KCl, 99.8%), formic acid (HCOOH, 88%), hydrogen chloride (HCl, 36% ~38%), potassium hydroxide (KOH, 85%), and acrylic acid (98%) were purchased from the Sinopharm Chemical Reagent Beijing Co., Ltd. (SCRC, China). All solutions were prepared with Milli-Q water (18.2 M Ω).

Nanochannel Preparation. The single asymmetric hourglass-shaped nanochannel investigated here was produced in a PET membrane (Hostaphan RN12 Hoechst, 19 μm thickness, with a single ion track in the center) by using a controllable asymmetric ion track-etching technique (see Test S1 and Figure S1, SI). Before asymmetric chemical etching, both sides of the tracked PET films were exposed to UV light for 1 h. To produce the asymmetric hourglass nanochannels with tunable shapes, etching was performed on both sides of the tracked PET films

with etchants of different concentrations: one side of the film was etched with 9 M NaOH, and the other side of the film was etched by 0 to 9 M NaOH. To monitor the etching process, a voltage (1 V) was applied on both sides of the PET film, and the transmembrane ionic current can be observed as soon as the nanochannel opens. After etching for a proper time, stopping solution (1 M KCl + 1 M HCOOH) was added to both sides of the cell to neutralize the etchant and thus stop the etching process.

Plasma-Induced Polymerization Method. The PET membrane should first be soaked in water overnight after the etching experiment. Only one side of the nanochannels was modified with PAA. Distilled acrylic acid (AAc) was injected into the plasma-induced grafting reactor (Suzhou Omega Machinery Electronic Technology Co., Ltd., DJ-02). The vacuum before switching on the glow discharge was 8 Pa, and the working temperature was 30 °C. The argon atmosphere was kept at about 50–60 Pa to glow discharge under 40 W, and this process lasted 15 min. After the glow extinguished, the grafting reactor would lead to the grafting of AAc monomers, and the vacuum

degree of 50–70 Pa was maintained. This would last about 15 min for the grafting reaction. After that, the chamber was connected with air. The plasma treatment was finished. At present, the experimental results of the asymmetric pH-gating ion transport properties of the nanochannels are indirect evidence for the asymmetric chemical modification of the nanochannels with pH-responsive PAA brushes.

Current Measurement. The ion transport properties of the nanochannel were studied by measuring ion current through the nanochannels before and after plasma treatment. Ion current was measured by a Keithley 6487 picoammeter (Keithley Instruments, Cleveland, OH, USA). A PET membrane, the center of which had a single nanochannel, was mounted between two chambers of the etching cell. Ag/AgCl electrodes were used to apply a transmembrane potential across the membrane. Forward voltage was the positive potential applied on the small base side of the nanochannel. The main transmembrane potential used in this work had been evaluated beforehand, and a scanning voltage varying from −2 to +2 V with a 40 s period was selected. The pH of the electrolyte was adjusted by 1 M HCl and KOH solutions, and the influence of addition substance quality can be ignored. It should be clear that all the pH values in this work are measured at 23 °C. All measurements were carried out in a custom-designed temperature control system. In this work, each test was repeated at least three times to obtain the average current value at different voltages on the same nanochannel.

Theoretical Simulation. Calculations of ion currents of the nanochannels before and after modification were performed using 2-D axial symmetries of the seven asymmetric hourglass geometries with different surface charge distributions (Figure S4 in the SI). All calculations were performed using MATLAB R2009b.

Conflict of Interest: The authors declare no competing financial interest.

Supporting Information Available: The Supporting Information is available free of charge on the ACS Publications website at DOI: 10.1021/acsnano.5b05542.

Fabrication of the asymmetric hourglass nanochannels, SEM images of cross sections of the nanochannels, conductance values of the single nanochannels before and after modification, surface charge distribution of the nanochannels before and after modification, details of the PNP model, parameters used for theoretical calculation (PDF)

Acknowledgment. This research is supported by the National Research Fund for Fundamental Key Projects (2011CB935700, 2013CB932802), National Natural Science Foundation (21501185, 21473213, 21201170, 11290163, 21421061, 91127025, 21171171), Key Research Program of the Chinese Academy of Sciences (KJZD-EW-M01, KJZD-EW-M03), and the 111 project. The authors thank the Material Science Group of GSI (Darmstadt, Germany) for providing the ion-irradiated samples.

REFERENCES AND NOTES

- Hille, B. *Ion Channels of Excitable Membranes*, 3rd ed.; Sinauer Associates: Sunderland, MA, 2001.
- Vlassiouk, I.; Siwy, Z. S. Nanofluidic Diode. *Nano Lett.* **2007**, *7*, 552–556.
- Jiang, Y.; Liu, N.; Guo, W.; Xia, F.; Jiang, L. Highly-Efficient Gating of Solid-State Nanochannels by DNA Supersandwich Structure Containing ATP Aptamers: A Nanofluidic Implication Logic Device. *J. Am. Chem. Soc.* **2012**, *134*, 15395–15401.
- Kalman, E. B.; Vlassiouk, I.; Siwy, Z. S. Nanofluidic Bipolar Transistors. *Adv. Mater.* **2008**, *20*, 293–297.
- Zeng, L.; Yang, Z.; Zhang, H.; Hou, X.; Tian, Y.; Yang, F.; Zhou, J.; Li, L.; Jiang, L. Tunable Ionic Transport Control inside a Bio-Inspired Constructive Bi-Channel Nanofluidic Device. *Small* **2014**, *10*, 793–801.
- Ali, M.; Mafe, S.; Ramirez, P.; Neumann, R.; Ensinger, W. Logic Gates Using Nanofluidic Diodes Based on Conical Nanopores Functionalized with Polyprotic Acid Chains. *Langmuir* **2009**, *25*, 11993–11997.
- Mafe, S.; Manzanares, J. A.; Ramirez, P. Gating of Nanopores: Modeling and Implementation of Logic Gates. *J. Phys. Chem. C* **2010**, *114*, 21287–21290.
- Ramirez, P.; Cervera, J.; Ali, M.; Ensinger, W.; Mafe, S. Logic Functions with Stimuli-Responsive Single Nanopores. *ChemElectroChem* **2014**, *1*, 698–705.
- Daigui, H. Ion Transport in Nanofluidic Channels. *Chem. Soc. Rev.* **2010**, *39*, 901–911.
- Martin, C. R.; Nishizawa, M.; Jirage, K.; Kang, M.; Lee, S. B. Controlling Ion-Transport Selectivity in Gold Nanotubule Membranes. *Adv. Mater.* **2001**, *13*, 1351–1362.
- Ali, M.; Yameen, B.; Cervera, J.; Ramirez, P.; Neumann, R.; Ensinger, W.; Knoll, W.; Azzaroni, O. Layer-by-Layer Assembly of Polyelectrolytes into Ionic Current Rectifying Solid-State Nanopores: Insights from Theory and Experiment. *J. Am. Chem. Soc.* **2010**, *132*, 8338–8348.
- Chen, W.; Wu, Z. Q.; Xia, X. H.; Xu, J. J.; Chen, H. Y. Anomalous Diffusion of Electrically Neutral Molecules in Charged Nanochannels. *Angew. Chem., Int. Ed.* **2010**, *49*, 7943–7947.
- Inglis, D. W.; Goldys, E. M.; Calander, N. P. Simultaneous Concentration and Separation of Proteins in a Nanochannel. *Angew. Chem., Int. Ed.* **2011**, *50*, 7546–7550.
- Kumar, B. V. V. S. P.; Rao, K. V.; Sampath, S.; George, S. J.; Eswaramoorthy, M. Supramolecular Gating of Ion Transport in Nanochannels. *Angew. Chem., Int. Ed.* **2014**, *53* (53), 13073–13077.
- Howorka, S.; Siwy, Z. Nanopore Analytics: Sensing of Single Molecules. *Chem. Soc. Rev.* **2009**, *38*, 2360–2384.
- Howorka, S.; Siwy, Z. S. Nanopores as Protein Sensors. *Nat. Biotechnol.* **2012**, *30*, 506–507.
- Miles, B. N.; Ivanov, A. P.; Wilson, K. A.; Dogan, F.; Japrung, D.; Edel, J. B. Single Molecule Sensing with Solid-State Nanopores: Novel Materials, Methods, and Applications. *Chem. Soc. Rev.* **2013**, *42*, 15–28.
- Cheng, L. J.; Guo, L. J. Nanofluidic Diodes. *Chem. Soc. Rev.* **2010**, *39*, 923–938.
- Eijkel, J. C. T.; van den Berg, A. Nanofluidics and the Chemical Potential Applied to Solvent and Solute Transport. *Chem. Soc. Rev.* **2010**, *39*, 957–973.
- Siwy, Z.; Trofin, L.; Kohli, P.; Baker, L. A.; Trautmann, C.; Martin, C. R. Protein Biosensors Based on Biofunctionalized Conical Gold Nanotubes. *J. Am. Chem. Soc.* **2005**, *127*, 5000–5001.
- Vlassiouk, I.; Kozel, T. R.; Siwy, Z. S. Biosensing with Nanofluidic Diodes. *J. Am. Chem. Soc.* **2009**, *131*, 8211–8220.
- de la Escosura-Muñiz, A.; Merkoçi, A. Nanochannels Preparation and Application in Biosensing. *ACS Nano* **2012**, *6*, 7556–7583.
- Siwy, Z.; Apel, P.; Baur, D.; Dobrev, D. D.; Korchev, Y. E.; Neumann, R.; Spohr, R.; Trautmann, C.; Voss, K. O. Preparation of Synthetic Nanopores with Transport Properties Analogous to Biological Channels. *Surf. Sci.* **2003**, *532*–535, 1061–1066.
- Lan, W. J.; Holden, D. A.; White, H. S. Pressure-Dependent Ion Current Rectification in Conical-Shaped Glass Nanopores. *J. Am. Chem. Soc.* **2011**, *133*, 13300–13303.
- Apel, P. Y.; Blonskaya, I. V.; Orelovitch, O. L.; Ramirez, P.; Sartowska, B. A. Effect of Nanopore Geometry on Ion Current Rectification. *Nanotechnology* **2011**, *22*, 175302.
- Fulinski, A.; Kosinska, I. D.; Siwy, Z. On the Validity of Continuous Modelling of Ion Transport through Nanochannels. *Europ. Lett.* **2004**, *67*, 683–689.
- Apel, P. Y.; Dmitriev, S. N.; Root, D.; Vutsadakis, V. A. A Novel Approach to Particle Track Etching: Surfactant Enhanced Control of Pore Morphology. *Phys. Part. Nucl. Lett.* **2000**, *4*, 69–74.
- Ali, M.; Ramirez, P.; Nguyen, H. Q.; Nasir, S.; Cervera, J.; Mafe, S.; Ensinger, W. Single Cigar-Shaped Nanopores Functionalized with Amphoteric Amino Acid Chains: Experimental and Theoretical Characterization. *ACS Nano* **2012**, *6*, 3631–3640.
- Kowalczyk, S. W.; Blosser, T. R.; Dekker, C. Biomimetic Nanopores: Learning from and About Nature. *Trends Biotechnol.* **2011**, *29*, 607–614.

30. Hou, X.; Guo, W.; Jiang, L. Biomimetic Smart Nanopores and Nanochannels. *Chem. Soc. Rev.* **2011**, *40*, 2385–2401.
31. Zhang, H. C.; Tian, Y.; Jiang, L. From Symmetric to Asymmetric Design of Bio-Inspired Smart Single Nanochannels. *Chem. Commun.* **2013**, *49*, 10048–10063.
32. Xia, F.; Guo, W.; Mao, Y.; Hou, X.; Xue, J.; Xia, H.; Wang, L.; Song, Y.; Ji, H.; Ouyang, Q.; Wang, Y.; Jiang, L. Gating of Single Synthetic Nanopores by Proton-Driven DNA Molecular Motors. *J. Am. Chem. Soc.* **2008**, *130*, 8345–8350.
33. Yameen, B.; Ali, M.; Neumann, R.; Ensinger, W.; Knoll, W.; Azzaroni, O. Single Conical Nanopores Displaying pH-Tunable Rectifying Characteristics. Manipulating Ionic Transport with Zwitterionic Polymer Brushes. *J. Am. Chem. Soc.* **2009**, *131*, 2070–2071.
34. Buchsbaum, S. F.; Nguyen, G.; Howorka, S.; Siwy, Z. S. DNA-Modified Polymer Pores Allow pH- and Voltage-Gated Control of Channel Flux. *J. Am. Chem. Soc.* **2014**, *136*, 9902–9905.
35. Zhang, H. C.; Hou, X.; Zeng, L.; Yang, F.; Li, L.; Yan, D. D.; Tian, Y.; Jiang, L. Bioinspired Artificial Single Ion Pump. *J. Am. Chem. Soc.* **2013**, *135*, 16102–16110.
36. Zhang, H. C.; Hou, X.; Hou, J.; Zeng, L.; Tian, Y.; Li, L.; Jiang, L. Synthetic Asymmetric-Shaped Nanodevices with Symmetric pH-Gating Characteristics. *Adv. Funct. Mater.* **2015**, *25*, 1102–1110.
37. Perez-Mittal, G.; Tuninetti, J. S.; Knoll, W.; Trautmann, C.; Toimil-Molares, M. E.; Azzaroni, O. Polydopamine Meets Solid-State Nanopores: A Bio-Inspired Integrative Surface Chemistry Approach to Tailor the Functional Properties of Nanofluidic Diodes. *J. Am. Chem. Soc.* **2015**, *137*, 6011–6017.
38. Zhu, X.; Liu, Y.; Huang, J.; Li, G. A pH-Responsive Gate Fabricated with Nanochannels and Nanoparticles. *Chem. - Eur. J.* **2010**, *16*, 1441–1444.
39. Liu, N.; Chen, Z.; Dunphy, D. R.; Jiang, Y.-B.; Assink, R. A.; Brinker, C. J. Photoresponsive Nanocomposite Formed by Self-Assembly of an Azobenzene-Modified Silane. *Angew. Chem., Int. Ed.* **2003**, *42*, 1731–1734.
40. Wang, G.; Bohaty, A. K.; Zharov, I.; White, H. S. Photon Gated Transport at the Glass Nanopore Electrode. *J. Am. Chem. Soc.* **2006**, *128*, 13553–13558.
41. Wen, L.; Liu, Q.; Ma, J.; Tian, Y.; Li, C.; Bo, Z.; Jiang, L. Malachite Green Derivative-Functionalized Single Nanochannel: Light-and-pH Dual-Driven Ionic Gating. *Adv. Mater.* **2012**, *24*, 6193–6198.
42. Xiao, K.; Xie, G.; Li, P.; Liu, Q.; Hou, G.; Zhang, Z.; Ma, J.; Tian, Y.; Wen, L.; Jiang, L. A Biomimetic Multi-Stimuli-Response Ionic Gate Using a Hydroxypyrene Derivation-Functionalized Asymmetric Single Nanochannel. *Adv. Mater.* **2014**, *26*, 6560–6565.
43. Yameen, B.; Ali, M.; Neumann, R.; Ensinger, W.; Knoll, W.; Azzaroni, O. Ionic Transport through Single Solid-State Nanopores Controlled with Thermally Nanoactuated Macromolecular Gates. *Small* **2009**, *5*, 1287–1291.
44. Zhang, L. X.; Cai, S. L.; Zheng, Y. B.; Cao, X. H.; Li, Y. Q. Smart Homopolymer Modification to Single Glass Conical Nanopore Channels: Dual-Stimuli-Actuated Highly Efficient Ion Gating. *Adv. Funct. Mater.* **2011**, *21*, 2103–2107.
45. Zhou, Y.; Guo, W.; Cheng, J.; Liu, Y.; Li, J.; Jiang, L. High-Temperature Gating of Solid-State Nanopores with Thermo-Responsive Macromolecular Nanoactuators in Ionic Liquids. *Adv. Mater.* **2012**, *24*, 962–967.
46. Hou, X.; Guo, W.; Xia, F.; Nie, F. Q.; Dong, H.; Tian, Y.; Wen, L. P.; Wang, L.; Cao, L. X.; Yang, Y.; Xue, J. M.; Song, Y. L.; Wang, Y. G.; Liu, D. S.; Jiang, L. A Biomimetic Potassium Responsive Nanochannel: G-Quadruplex DNA Conformational Switching in a Synthetic Nanopore. *J. Am. Chem. Soc.* **2009**, *131*, 7800–7805.
47. Liu, Z.; Luo, F.; Ju, X. J.; Xie, R.; Luo, T.; Sun, Y. M.; Chu, L. Y. Positively K+-Responsive Membranes with Functional Gates Driven by Host–Guest Molecular Recognition. *Adv. Funct. Mater.* **2012**, *22*, 4742–4750.
48. Tian, Y.; Zhang, Z.; Wen, L.; Ma, J.; Zhang, Y.; Liu, W.; Zhai, J.; Jiang, L. A Biomimetic Mercury(II)-Gated Single Nanochannel. *Chem. Commun.* **2013**, *49*, 10679–10681.
49. Liu, Q.; Xiao, K.; Wen, L.; Dong, Y.; Xie, G.; Zhang, Z.; Bo, Z.; Jiang, L. A Fluoride-Driven Ionic Gate Based on a 4-Aminophenylboronic Acid-Functionalized Asymmetric Single Nanochannel. *ACS Nano* **2014**, *8*, 12292–12299.
50. Zhu, X.; Zhang, B.; Ye, Z.; Shi, H.; Shen, Y.; Li, G. An ATP-Responsive Smart Gate Fabricated with a Graphene Oxide-Aptamer-Nanochannel Architecture. *Chem. Commun.* **2015**, *51*, 640–643.
51. Hou, X.; Zhang, H.; Jiang, L. Building Bio-Inspired Artificial Functional Nanochannels: From Symmetric to Asymmetric Modification. *Angew. Chem., Int. Ed.* **2012**, *51*, 5296–5307.
52. Cuello, L. G.; Romero, J. G.; Cortes, D. M.; Perozo, E. pH-Dependent Gating in the Streptomyces Lividans K⁺ Channel. *Biochemistry* **1998**, *37*, 3229–3236.
53. MacKinnon, R. Potassium Channels and the Atomic Basis of Selective Ion Conduction (Nobel Lecture). *Angew. Chem., Int. Ed.* **2004**, *43*, 4265–4277.
54. Nanazashvili, M.; Li, H.; Palmer, L. G.; Walters, D. E.; Sackin, H. Moving the Ph Gate of the Kir1.1 Inward Rectifier Channel. *Channels* **2007**, *1*, 22–29.
55. Zhang, H. C.; Hou, X.; Yang, Z.; Yan, D.; Li, L.; Tian, Y.; Wang, H.; Jiang, L. Bio-Inspired Smart Single Asymmetric Hourglass Nanochannels for Continuous Shape and Ion Transport Control. *Small* **2015**, *11*, 786–791.
56. Wolf, A.; Reber, N.; Apel, P. Y.; Fischer, B. E.; Spohr, R. Electrolyte Transport in Charged Single Ion Track Capillaries. *Nucl. Instrum. Methods Phys. Res., Sect. B* **1995**, *105*, 291–293.
57. Siwy, Z.; Apel, P.; Dobrev, D.; Neumann, R.; Spohr, R.; Trautmann, C.; Voss, K. Ion Transport through Asymmetric Nanopores Prepared by Ion Track Etching. *Nucl. Instrum. Methods Phys. Res., Sect. B* **2003**, *208*, 143–148.
58. Hou, X.; Liu, Y.; Dong, H.; Yang, F.; Li, L.; Jiang, L. A pH-Gating Ionic Transport Nanodevice: Asymmetric Chemical Modification of Single Nanochannels. *Adv. Mater.* **2010**, *22*, 2440–2443.
59. Cervera, J.; Schiedt, B.; Neumann, R.; Mafe, S.; Ramirez, P. Ionic Conduction, Rectification, and Selectivity in Single Conical Nanopores. *J. Chem. Phys.* **2006**, *124*, 104706–104709.
60. Kosinska, I. D.; Goychuk, I.; Kostur, M.; Schmid, G.; Hanggi, P. Rectification in Synthetic Conical Nanopores: A One-Dimensional Poisson-Nernst-Planck Model. *Phys. Rev. E* **2008**, *77*, 031131.
61. Tagliazucchi, M.; Rabin, Y.; Szleifer, I. Transport Rectification in Nanopores with Outer Membranes Modified with Surface Charges and Polyelectrolytes. *ACS Nano* **2013**, *7*, 9085–9097.
62. Tagliazucchi, M.; Rabin, Y.; Szleifer, I. Ion Transport and Molecular Organization Are Coupled in Polyelectrolyte-Modified Nanopores. *J. Am. Chem. Soc.* **2011**, *133*, 17753–17763.